Research Square

Preprints are preliminary reports that have not undergone peer review.
They should not be considered conclusive, used to inform clinical practice,
or referenced by the media as validated information.

Multi-Modal Fusion of Olfactory and Visual Features for Precise Mango Maturity Classification

Liu Yang
yangliuvictry@whpu.edu.cn
Wuhan Polytechnic University
Zhiwei Liu
Wuhan Polytechnic University
Junfeng Wu
Wuhan Polytechnic University
Menghao Zhao
Wuhan Polytechnic University
Pingan Huang
Wuhan Polytechnic University
Jiaming Wang
Wuhan Polytechnic University
Can Shu
Wuhan Polytechnic University
Xinfeng Hu
Wuhan Polytechnic University
Shaoyun Song
Wuhan Polytechnic University

Research Article

Keywords: Mango maturity assessment, Multi-modal fusion, Computer vision, Gas-sensing array, PCA-Logistic model

Posted Date: May 11th, 2026

DOI: https://doi.org/10.21203/rs.3.rs-9353259/v1

License: This work is licensed under a Creative Commons Attribution 4.0 International License. Read Full License

Additional Declarations: No competing interests reported.

Abstract

Precise assessment of mango maturity is vital for minimizing postharvest losses. This study proposes a multi-modal recognition method combining gas-sensing and image features to classify mangoes into four stages: mature green (MG), color break (CB), mature (M), and over-mature (OM). A custom multi-channel gas detection system and image processing techniques were employed to extract olfactory and HSV color features. The 14-dimensional feature set was reduced using Principal Component Analysis (PCA), yielding three principal components (PCs) that retained 91.01% of the total variance. A PCA-Logistic Maturity Classification (PLMC) model was subsequently constructed and exhibited an excellent fit ($p < 0.01$). Analysis revealed that PC1 (gas-sensing parameters) played a dominant role, with odds ratios (ORs) significantly increasing from 2.28 (CB) to 16.70 (OM). PC2 (hue-brightness) strongly indicated early ripening (OR = 2.64 for CB), while PC3 (saturation) had minimal impact. The PLMC model achieved a 98% overall accuracy, perfectly identifying MG and OM stages (100%), and reaching 96% for CB and M stages. By overcoming the limitations of single-sensor approaches, this data fusion method provides a reliable technical foundation for automated and non-destructive fruit grading.

1. Introduction

Driven by economic development and rising living standards, consumer demand for high-quality, flavorful fresh produce has surged significantly (Mason-D'Croz et al., 2019; Li et al., 2022). Mango, a highly favored tropical fruit, is globally renowned for its distinctive aroma, desirable taste, and rich nutritional profile (Chay et al., 2019; Chakraborty et al., 2020). However, as a typical climacteric fruit, mangoes exhibit a rapid increase in respiration rates post-harvest. This physiological process accelerates flesh softening and the release of volatile organic compounds (Paul et al., 2019). If the optimal harvest window or sales period is missed, mangoes are highly susceptible to overripening and decay, leading to severe economic consequences (Liu et al., 2023). Current data indicates that postharvest losses of mangoes can reach up to 20% (Ntsoane et al., 2019). Traditionally, the quality and maturity assessment of mangoes heavily relies on human sensory panels (Huang et al., 2018). Such subjective evaluations are inherently limited by individual experience, visual fatigue, and environmental factors, making the accurate and consistent assessment of mango maturity a critical bottleneck in the fruit supply chain (Mim et al., 2018; Patil and Parray, 2024).

To address these limitations, recent research has increasingly shifted toward non-destructive and intelligent detection methods, primarily leveraging computer vision and machine learning. Numerous studies have focused on image-based grading systems. For instance, Worasawate et al. (2022) and Supekar et al. (2020) utilized artificial neural networks and clustering algorithms to classify mango ripeness based on external features like color and shape. More recently, advanced deep learning models, such as Xception (Ballo et al., 2024) and CNN architectures like VGG16 (Islam et al., 2025), have been deployed to extract complex visual traits, demonstrating impressive image recognition performance. Despite these advancements, image-based approaches possess inherent limitations: they primarily capture surface characteristics and are highly sensitive to lighting conditions, shooting angles, and cultivar variations (Ntsoane et al., 2019; Singh et al., 2025). Because they lack the ability to detect internal biochemical changes, visual methods alone struggle to fully determine true maturity. To capture internal traits, researchers have explored alternative sensors. Neto et al. (2025) applied electrical impedance spectroscopy to monitor internal tissue changes, while Huang et al. (2018) and Li et al. (2024) demonstrated the benefits of fusing computer vision with colorimetric or impedance sensors to enhance classification robustness. Similarly, while electronic nose (gas-sensing) technology can effectively detect internal volatile emissions representing ripeness, it completely ignores external visual cues (e.g., peel color) and is vulnerable to complex background odors. Consequently, relying on a single detection modality often forces a compromise between accuracy and environmental robustness, particularly when subtle color shifts or minor odor differences occur during the transitional stages of ripening.

To overcome the inherent limitations of single-modal detection, this study proposes a novel multi-source feature recognition method that fuses gas-sensing data with image properties. Using Hainan Xiaotai mangoes as the research subject, gas-sensing responses (Wilson et al., 2009; Voss et al., 2019) and visual features (Hue, Saturation, and Value

channels) (Salunkhe et al., 2015) were systematically collected across four distinct maturity stages. Following data standardization, a fused feature matrix was constructed. Principal Component Analysis (PCA) was employed to reduce dimensionality and extract the most representative variables (Hasan et al., 2021). Subsequently, a PCA-Logistic Maturity Classification (PLMC) model was developed, utilizing the extracted principal components to predict maturity stages. The robustness and predictive capability of the PLMC model were rigorously evaluated using the likelihood ratio test, Wald test, and classification matrices. By seamlessly integrating internal olfactory signals with external visual features, this approach eliminates the blind spots of single-sensor methods, providing a reliable, cost-effective, and innovative technical foundation for the non-destructive online monitoring and intelligent sorting of tropical fruits.

2. Material and methods

2.1 Materials and sample preparation

'Xiaotai' mangoes (Mangifera indica L.) harvested from Hainan Province, China, were used as the experimental subjects. The mango samples had a mass ranging from 70 to 130 g, with an average length and width of 67.94 ± 7.47 mm and 44.76 ± 4.92 mm, respectively (Fig. 1A). Following harvest, the mangoes were immediately transported to the laboratory via a cold-chain logistics system. To maintain stable respiration rates and preserve volatile profiles, the samples were stored in a constant temperature and humidity chamber (KHWS-400, Kenton, China) at 13 ± 1°C and a relative humidity (RH) of 60 ± 1% (Lufu et al., 2019).

According to the Chinese agricultural standard DB46/T 173–2009, combined with literature criteria (Shah et al., 2021; Busatto et al., 2022), the mangoes were classified into four distinct maturity stages: mature green (MG), color break (CB), mature (M), and over-mature (OM). The physical characteristics of these stages are described as follows (Fig. 1B): at the MG stage, the peel was dark green and the flesh remained firm; at the CB stage, the peel transitioned from green to yellow, initiating flesh softening; at the M stage, the skin exhibited extensive yellow coloration accompanied by moderate flesh softening; and at the OM stage, the flesh became excessively soft, the peel turned entirely yellow, and brown necrotic spots began to develop.

The experimental hardware setup primarily consisted of a commercial electronic nose (CNOSE-28), a custom-built gas-sensing detection platform (Fig. 2A), a high-definition camera (1920 × 1080 pixels) for image acquisition, vernier calipers, miniature air pumps, three-way valves, and an electronic balance. Initially, the CNOSE-28 electronic nose was employed to screen and select the optimal gas sensors. For the custom platform, an STM32F103C8T6 microcontroller served as the core control module, while LabVIEW was utilized as the host software to facilitate real-time data acquisition and system control. Both the mango sampling chamber and the sensor array chamber were fabricated using 3D printing technology. The specific models and target gases of the selected sensors are detailed in Table 1.

Table 1
Sensors types and main response gases

Type of sensor	Main response gas
MQ137	Ammonia, organic amines, etc
MQ135	Ammonia, sulphide, benzene, etc
MQ136	Sulfides, etc.
MQ138	Organic vapours such as toluene, acetone and ethanol
MQ5	Combustible gases such as methane, propane and butane
MQ4	Methane, natural gas, etc
MQ3	Alcohols such as ethanol
TGS2620	Ethanol, organic solvents, etc

2.2 Experimental procedure and data acquisition

The experimental workflow consisted of two parallel phases: gas-sensing detection and image feature extraction. Figure 2B illustrates the overall schematic of the gas-sensing process. During the gas-sensing detection phase, individual mango samples were placed into the sampling chamber of a custom-built multi-channel MOS sensor platform. The chamber was sealed for a specific duration to allow the headspace volatile organic compounds (VOCs) to reach equilibrium. Subsequently, the inlet valve was opened, and a miniature air pump was activated to transfer the equilibrated headspace gas into the sensor array chamber. Real-time sensor response curves were continuously acquired and visualized via LabVIEW software on a host PC (Fig. 2C). The steady-state response of each channel was extracted and recorded as the characteristic olfactory value for the respective sample. Following each measurement cycle, the three-way valve was switched to draw in filtered ambient air, thoroughly purging the sensor chamber to recover the baseline in preparation for the subsequent test.

Concurrently, in the image feature extraction phase, surface images of the mangoes were captured under a standardized and uniform illumination setup. The acquired images were cropped to define the region of interest (ROI), denoised, and subjected to white-balance correction to minimize environmental interference (Surya et al., 2015). Finally, the preprocessed images were transformed from the RGB color space into the Hue, Saturation, and Value (HSV) color space. The mean and standard deviation of each HSV channel were then calculated to construct the visual feature dataset.

2.3 Statistical analysis

All data processing and statistical modeling were performed using SPSS software. Prior to analysis, missing values were handled using the median imputation method, and outliers were identified and addressed via the interquartile range (IQR) rule to ensure data quality. The extracted gas-sensing and image feature sets were standardized using the Z-score method to eliminate dimensional discrepancies and then concatenated into a fused multi-source feature matrix.

Principal Component Analysis (PCA) was applied to this matrix for dimensionality reduction. According to Kaiser’s criterion, three principal components (PCs) with eigenvalues greater than 1 were retained, and the corresponding component scores for each sample were calculated. Subsequently, a PCA-Logistic Maturity Classification (PLMC) model was constructed. The three retained PC scores served as the independent variables, while the categorical maturity stage labels acted as the dependent variable, with the MG (mature green) stage designated as the reference category. The predictive performance and goodness-of-fit of the PLMC model were rigorously evaluated through the likelihood ratio test, Wald test parameter estimates, and overall classification accuracy matrices.

3. Results and discussion

3.1 Evolution of gas-sensing features across maturity stages

A total of 100 'Xiaotai' mango samples (25 samples per maturity stage: MG, CB, M, and OM) were analyzed using the custom-built multi-channel MOS sensor platform. To ensure measurement reliability, the steady-state peak of each sensor channel was extracted in triplicate. As illustrated in Fig. 3, the steady-state responses of all eight sensors exhibited a continuous upward trend from the MG stage to the OM stage. This macroscopic trend aligns precisely with the progressive accumulation and release of volatile organic compounds (VOCs) during the ripening process of climacteric fruits.

The evolution of the gas-sensing responses can be distinctly divided into stage-specific patterns. During the transition from the MG to the CB stage, the sensor responses entered their initial rapid growth phase. Notably, the response of MQ135 surged by 77.1% (from 175 to 310), and TGS2620 increased by 33.0% (from 545 to 725). Other sensors, such as MQ3, MQ4, and MQ5, demonstrated moderate increases of 20–30%, whereas MQ137 showed a slight increase of 8.6%. This rapid overall elevation likely reflects the sharp surge in ethanol and amine emissions associated with the onset of the respiratory climacteric peak (Zakaria et al., 2012).

As the fruit progressed from the CB to the M stage, VOC emissions reached a period of intense accumulation. During this phase, sensors highly sensitive to terpenes and sulfides-specifically MQ136, MQ137, and MQ138-exhibited the most substantial growth. For instance, the response of MQ3 increased dramatically by 37.6% (from 1900 to 2615). These findings are highly consistent with previous reports indicating a marked increase in the synthesis of alcohols and terpenoid compounds when mangoes reach full maturity (Tang et al., 2010).

Conversely, during the transition from the M to the OM stage, the growth rates of the sensor responses decelerated significantly. The response of MQ137 increased only marginally by 5.8% (from 3700 to 3915), while the growth rates for MQ135 and MQ3 dropped to less than 10%. This plateauing trend suggests a deceleration in new VOC synthesis and the more dispersed diffusion of gases following severe cell-wall degradation and tissue senescence (Wilson et al., 2009).

In summary, the step-wise evolution of VOC emissions-characterized by distinct physiological nodes at the CB stage (climacteric initiation) and the M stage (volatile accumulation)-validates that the multi-channel MOS array can capture the internal biochemical shifts of the fruit. This provides highly reliable olfactory markers for the online monitoring of mango maturity.

3.2 Evolution of visual characteristics across maturity stages

The quantitative visual features of the mangoes, extracted from the preprocessed images and represented by the mean and standard deviation of the Hue (H), Saturation (S), and Value (V) channels, are summarized in Table 2.

Table 2
Mango image features at different maturity stages

Maturity stage	H channel mean value	H channel standard deviation	S channel mean value	S channel standard deviation	V channel mean value	V channel standard deviation
Mature green	32.53	3.78	57.74	5.41	155.24	14.05
Color break	28.83	3.77	66.70	10.94	162.72	20.85
maturity	26.92	1.45	71.56	8.94	164.29	4.75
Over-maturity	26.86	2.03	65.51	13.97	157.10	3.30

At the initial MG stage, the high chlorophyll content in the peel endowed the mangoes with a deep green appearance, which quantitatively corresponded to the highest mean Hue (H) value of 32.53. Both Saturation (S) and Value/brightness (V) remained at relatively moderate levels (57.74 and 155.24, respectively). As ripening progressed into the CB stage, a distinct chromatic transition from green to yellow-green occurred. This phase was characterized by an 11.4% decrease in the mean H value (down to 28.83), alongside notable increases in S (to 66.70) and V (to 162.72). These dynamic shifts are primarily driven by the rapid degradation of chlorophyll coupled with the onset of carotenoid synthesis, which collectively enhance the color purity and brightness of the fruit.

Upon reaching full maturity (the M stage), the accumulation of carotenoids peaked, producing a vivid golden-yellow peel. This physiological peak was visually captured by the maximization of both mean S (71.56) and mean V (164.29). Crucially, as shown in Table 2, the standard deviations of the H and V channels at the M stage dropped to their absolute minimums (1.45 and 4.75, respectively). This sharp decrease in variance mathematically demonstrates that the skin coloration becomes highly uniform across the fruit surface at optimal ripeness.

Conversely, during the transition to the OM stage, while the fundamental Hue remained relatively stable (26.86), both S and V exhibited noticeable declines, dropping by 8.4% (to 65.51) and 4.4% (to 157.10), respectively. This reduction in color intensity and surface gloss is a direct visual manifestation of tissue senescence, cellular breakdown, and enzymatic browning (Pathare et al., 2013). Furthermore, the standard deviation of the S channel surged to 13.97 during the OM stage, a statistical reflection of the uneven development of brown necrotic spots and localized decay on the over-mature peel.

The extracted HSV parameters effectively quantify the dynamic, stage-specific color evolution of mangoes. These visual trajectories provide a robust, non-destructive dataset that perfectly complements the internal olfactory features, establishing a comprehensive foundation for the proposed multi-modal maturity discrimination model.

3.3 PCA dimensionality reduction analysis

To eliminate information redundancy among the multi-source data, Principal Component Analysis (PCA) was performed on the standardized 14-dimensional feature matrix. As summarized in Table 3, based on Kaiser's criterion (eigenvalues > 1), the first three principal components (PCs) were retained. Specifically, PC1, PC2, and PC3 yielded eigenvalues of 8.626, 2.716, and 1.399, accounting for 61.61%, 19.40%, and 9.99% of the total variance, respectively. Cumulatively, these three components capture 91.01% of the original dataset's variance, indicating that they adequately represent the comprehensive multi-source feature set with minimal information loss.

Table 3
Principal component eigenvalue and contribution rate

Component	Initial eigenvalues			Extraction sum squares loads			Rotated sum squares loads		
	Total	variance %	Cumulative %	Total	variance %	Cumulative %	Total	variance %	Cumulative %
1	8.626	61.613	61.613	8.626	61.613	61.613	7.786	55.614	55.614
2	2.716	19.401	81.014	2.716	19.401	81.014	2.864	20.457	76.071
3	1.399	9.994	91.008	1.399	9.994	91.008	2.091	14.937	91.008
4	0.618	4.415	95.423						
5	0.25	1.788	97.211						
6	0.154	1.102	98.313						
7	0.083	0.593	98.906						
8	0.068	0.486	99.391						
9	0.03	0.217	99.608						
10	0.023	0.163	99.771						
11	0.017	0.121	99.892						
12	0.009	0.064	99.956						
13	0.004	0.029	99.985						
14	0.002	0.015	100						

To enhance the physical interpretability of the extracted components, a Varimax orthogonal rotation was applied. As displayed in Table 4, the rotated component loading matrix maps the original variables to the new PC space. Notably, PC1 exhibited exceptionally high positive loadings (> 0.94) across all gas-sensing channels, clearly representing the "olfactory/gas-sensing factor." PC2 demonstrated strong correlations with the visual H channel (loading = − 0.72) and V channel (loading = 0.97), signifying peel hue and brightness, respectively; thus, it was designated as the "hue-brightness factor." PC3 was predominantly driven by the S channel (loading = 0.96), functioning as the "saturation factor." This decoupled representation of chemical (odor) and physical (color) traits provides a robust, highly interpretable, and low-dimensional input basis for the subsequent PLMC model.

Table 4
Rotated component matrix

Initial independent variable	component		
Principal components	1	2	3
MQ137	0.94		
MQ3	0.98		
MQ135	0.98		
MQ136	0.96		
MQ138	0.95		
MQ5	0.93		
MQ4	0.95		
TGS2620	0.98		
H channel mean value		-0.72	
H channel standard deviation		0.83	
S channel mean value			0.96
S channel standard deviation			0.87
V channel mean value		0.97	
V channel standard deviation		-0.82	

To facilitate visualization and evaluate the natural clustering tendency of the samples, a 2D scatter plot was generated using the two most dominant components, PC1 and PC2 (Fig. 4). The plot reveals distinct spatial separation among the four maturity stages, perfectly mirroring their physiological changes. At the MG stage, samples are clustered tightly in the lower-left quadrant (low PC1 and low PC2 scores), reflecting their minimal volatile emissions and dark green, low-brightness appearance. As the mangoes progress to the CB stage, the cluster shifts rightward and upward; the PC1 scores increase to approximately − 0.5, and PC2 scores rise towards 0. This shift mathematically captures the initiation of VOC release and the lightening of the peel.

At the fully mature (M) stage, the samples advance further along both axes, occupying regions with higher PC1 scores (> 0) and peak PC2 scores (around 0). This coordinate position indicates robust aromatic volatile accumulation and maximum visual brightness, corresponding to the characteristic golden-yellow appearance of ripe mangoes. Finally, at the OM stage, the samples shift to the extreme right (highest PC1 scores, typically > 1.5), confirming the intense release of senescence-related volatiles (e.g., ethanol from anaerobic fermentation). Concurrently, their PC2 scores exhibit a noticeable decline compared to the M stage. This downward shift in the PC2 axis accurately captures the loss of surface gloss and the emergence of dull, necrotic brown spots on over-mature skin. Ultimately, the distinct boundaries between these clusters-particularly the maximum spatial separation between the MG and OM stages-demonstrate the exceptional efficacy of PCA in characterizing maturity progression, laying a solid foundation for the classification model.

3.4 PLMC model construction and classification performance

To quantitatively classify the ripening stages based on the fused multimodal data, a PCA-Logistic Maturity Classification (PLMC) model was constructed. A multinomial logistic regression algorithm was employed, utilizing the three extracted principal component scores (PC1, PC2, and PC3) as independent predictors and the maturity category (Y) as the dependent

variable. The mature green (MG, Y = 0) stage was designated as the baseline reference category. All model parameters were optimized via the maximum likelihood estimation (MLE) method.

The overall goodness-of-fit for the proposed PLMC model is summarized in Table 5. Upon incorporating the three principal components, the − 2 Log-Likelihood value exhibited a substantial decrease from the intercept-only baseline of 109.89 to 69.93. This reduction yielded a highly significant likelihood ratio test statistic (\chi^2(9) = 39.97, p < 0.01), confirming that the integration of the fused PCA features fundamentally improved the explanatory power of the model. Furthermore, the McFadden pseudo-R^2 value reached 0.64, indicating a robust fit and excellent predictive capacity for maturity classification.

Table 5
Goodness-of-fit test results

Model	**the model Fitting conditions**	**Likelihood ratio test**		
	-2 log-likelihood	**Chi-square**	**Degrees of freedom**	**Significance**
Intercept only	109.89			
Final	69.93	39.97	9	0.01

To interpret the physiological drivers behind the model, the parameter estimates and odds ratios (OR, expressed as Exp(B)) were evaluated via the Wald test, as detailed in Table 6. Notably, all retained principal components demonstrated statistical significance (p < 0.05) across the transition stages.

Table 6
Estimated parameters table

Maturity		**B**	**Standard error**	**Significance**	**Exp(B)**	**95% confidence interval for EXP (b)**
Color break	Intercept	-1.93	1.299	0.035		
	PCA1	0.825	0.322	0.012	2.282	[1.217, 4.278]
	PCA2	0.97	0.22	0.036	2.638	[1.712, 4.063]
	PCA3	-0.02	0.021	0.042	0.98	[0.940, 1.023]
maturity	Intercept	-1.564	1.002	0.005		
	PCA1	1.32	0.451	0.003	3.743	[1.544, 9.076]
	PCA2	0.567	0.434	0.032	1.763	[0.752, 4.132]
	PCA3	-0.095	0.049	0.043	0.909	[0.825, 1.002]
Over-maturity	Intercept	-2.681	1.979	0.006		
	PCA1	2.814	0.375	0.001	16.7	[8.165, 34.159]
	PCA2	-0.135	0.26	0.004	0.874	[0.525, 1.451]
	PCA3	-0.134	0.029	0.024	0.875	[0.825, 0.928]

The Olfactory Factor (PC1) emerged as the dominant discriminator throughout the entire ripening lifecycle. The ORs for PC1 increased exponentially as maturity progressed: 2.282 for the CB stage, 3.743 for the M stage, and a staggering 16.70 for the OM stage. This confirms that the continuous, massive accumulation of internal VOC emissions (captured by the gas-sensing array) is the absolute core indicator driving the probability of a mango transitioning into advanced maturity.

The Hue-Brightness Factor (PC2) exhibited bidirectional behavior perfectly aligned with visual physiology. During the early and middle stages, PC2 had a significant positive effect (OR = 2.638 for CB; 1.763 for M), indicating that the lightening and yellowing of the peel facilitate early maturity detection. Conversely, at the OM stage, PC2 displayed a significant negative effect (B = -0.135, p = 0.004, OR = 0.874). This statistical reversal accurately captures the senescence phase, where the emergence of necrotic brown spots and the loss of surface gloss drastically reduce image brightness.

The Saturation Factor (PC3) acted as a supplementary discriminative variable. Its odds ratios hovered slightly below 1 across all stages, exerting a subtle negative regulatory effect that assists in refining the boundary between the M and OM categories.

These parameter dynamics profoundly validate that while gas-sensing (PC1) establishes the foundational maturity baseline, image features (PC2, PC3) provide critical supplementary geometric boundaries, making the multimodal fusion vastly superior to single-sensor approaches.

Finally, the classification efficacy of the PLMC model was evaluated using a balanced dataset (n = 100, 25 samples per stage). As presented in the prediction matrix (Table 7), the model achieved an exceptional overall classification accuracy of 98.00%. Specifically, the model demonstrated flawless performance (100% accuracy) for the extreme categories, MG and OM. The minimal misclassifications occurred exclusively between adjacent transitional phases: one CB sample was misclassified as M, and one M sample was misclassified as OM. Biologically, this is highly reasonable, as fruit ripening is a continuous biochemical continuum rather than a set of discrete leaps, making boundary samples inherently ambiguous. Ultimately, the PLMC model's precise discrimination, especially its ability to differentiate the easily confused M and OM stages, validates its immense potential and reliability for automated, online mango grading systems.

Table 7
Mango maturity classification and prediction table

Prediction / **Measured**	**Mature green**	**Color break**	**Maturity**	**Over-maturity**	**Accuracy**
Mature green	25	0	0	0	100.00%
Color break	0	24	1	0	96.00%
Maturity	0	0	24	1	96.00%
Over-maturity	0	0	0	25	100.00%
Overall percentage	25.00%	24.00%	25.00%	26.00%	98.00%

4. Conclusions

In this study, a novel non-destructive, multi-modal recognition framework was successfully developed for the precise classification of mango maturity by synergistically integrating gas-sensing arrays and computer vision. By extracting steady-state olfactory signals and HSV color features across four ripening stages (MG, CB, M, and OM), a 14-dimensional feature matrix was established. Dimensionality reduction via PCA successfully decoupled the complex dataset into three interpretable principal components, capturing 91.01% of the cumulative variance.

The subsequently constructed PCA-Logistic Maturity Classification (PLMC) model elucidated the distinct physiological roles of these multi-source features during the ripening process. Statistical analysis confirmed that the olfactory factor (PC1) serves as the absolute dominant discriminant, reflecting the exponential accumulation of volatile organic compounds (VOCs) as the fruit progresses toward senescence. Meanwhile, the visual features acted as essential complementary discriminators: the hue-brightness factor (PC2) effectively captured the critical skin color transitions during

the early and middle stages (CB and M), whereas the saturation factor (PC3) provided the necessary boundary constraints to accurately distinguish between optimal maturity and over-maturity (M vs. OM).

Ultimately, the PLMC model achieved an outstanding overall classification accuracy of 98.0%. It demonstrated flawless identification (100%) for the extreme MG and OM stages, and robust discrimination (96%) for the highly confusable transitional phases (CB and M). These findings conclusively demonstrate that fusing internal biochemical signals with external physical traits overcomes the inherent blind spots of single-sensor approaches. The proposed multi-source fusion method provides a highly reliable, cost-effective, and interpretable technical foundation for the automated online grading and intelligent postharvest management of tropical fruits.

Declarations

AUTHOR CONTRIBUTIONS

Liu Yang: Conceptualization; funding; writing-review & editing. **Zhiwei Liu:** Investigation; writing-original draft preparation; materials characterization, methodology. **Junfeng Wu:** Experimental assistance. **Menghao Zhao:** Experimental assistance. **Pingan Huang:** Data analysis, experimental assistance, review & editing. **Jiaming Wang:** Experimental assistance. **Can Shu:** Experimental assistance. **Xinfeng Hu:** Collaboration; review & editing. **Shaoyun Song:** Supervision; review & editing

ACKNOWLEDGMENTS

The study is mainly funded by the Science and technology research project of Hubei Grain Bureau (2023HBLSKJ005), the Youth Project of Nature Science Foundation of Hubei Province (No. 2022CFB944), Science and Technology Research Project of Hubei Provincial Education Department (No. Q20211609), Key R&D plan of Hubei Province (No. 2022BBA0047), part of the research is supported by Jiangsu Key Laboratory of Advanced Food Manufacturing Equipment & Technology (FM-202103)

CONFLICT OF INTEREST STATEMENT

The authors declare no conflicts of interest.

DATA AVAILABILITY STATEMENT

The data support the findings of this study are available from the corresponding author upon reasonable request.

ETHICS STATEMENT

This study does not involve any human or animal testing.

INFORMED CONSENT STATEMENT

Written informed consent was obtained from all study participants.

ORCID

Liu Yang https://orcid.org/0000-0002-1922-4501

References

1. Bogard M-DD, Sulser JR, Cenacchi TB, Nicola, Dunston, Shahnila, Herrero, Mario, and, Wiebe K (2019) Gaps between fruit and vegetable production, demand, and recommended consumption at global and national levels: an integrated modelling study. The Lancet Planetary Health 3(7): e318-e329

2. Li X, Jiahao CBL Y., et al (2022) Trends and Challenges on Fruit and Vegetable Processing: Insights into Sustainable, Traceable, Precise, Healthy, Intelligent, Personalized and Local Innovative Food Products. Trends Food Sci Technol 125:12–25
3. Chay KG, Workeneh A, Shifera B (2019) A review on production and marketing of mango fruit. World J Agric Soil Sci 2(2):1–7
4. Chakraborty R, Roy S, Mondal P (2020) Quartz halogen radiated fast and energy-efficient convective vacuum drying of green tea fortified Himsagar mango: Optimization, kinetics, and quality assessment. J Food Process Eng 43(8):e13441
5. Paul V, Pandey R, Malik SK (2019) Varietal variations in rate of ripening and respiration of mango (Mangifera indica L.) fruits: anatomical substantiation. Plant Physiol Rep 24:340–350
6. Liu B, Xin Q, Zhang M, Chen J, Lu Q, Zhou X, Li X, Zhang W, Feng W, Pei H, Sun J (2023) Research Progress on Mango Post-Harvest Ripening Physiology and the Regulatory Technologies. Foods 12(1):173
7. Ntsoane ML, Zude-Sasse M, Mahajan P et al (2019) Quality assessment and postharvest technology of mango: A review of its current status and future perspectives. Sci Hort 249:77–85
8. Huang X, Lv R, Wang S, Aheto JH, Dai C (2018) Integration of computer vision and colorimetric sensor array for nondestructive detection of mango quality. J Food Process Eng 41(8):e12873
9. Patil RK, Parray RA (2024) Advancing Mango Ripeness Assessment: A Comprehensive Study Integrating VNIR Spectroscopy and SIMCA Modelling for 'Dashehari' Cultivar. Eur J Nutr Food Saf 16(3):27–34
10. Mim FS, Galib SM, Hasan MF et al (2018) Automatic detection of mango ripening stages: An application of information technology to botany. Sci Hort 237:156–163
11. Worasawate D, Sakunasinha P, Chiangga S (2022) Automatic classification of the ripeness stage of mango fruit using a machine learning approach. *AgriEngineering* 4(1): 32–47
12. Supekar AD, Wakode M (2020) Multi-parameter based mango grading using image processing and machine learning techniques. INFOCOMP J Comput Sci 19(2):175–187
13. Abou BB, Moustapha D, Adama C (2024) An application of machine learning methods to detect mango varieties. Open J Appl Sci 14(7):1666–1690
14. Islam MS, Islam M (2025) Improving mango ripeness grading accuracy: A comprehensive analysis of deep learning, traditional machine learning, and transfer learning techniques. Mach Learn Appl 19:100619
15. Neto AF, Silva RJ, Pereira SB (2025) Electrical impedance spectroscopy in agricultural food: Application to mango maturity measurement. J Food Process Eng 48(3):e70085
16. Li X, Zhang Y, Chen L (2024) Non-destructive grading technique for mangoes using a flexible impedance sensing system and YOLOv5s + CBAM. J Food Process Eng 47(5):e14631
17. Singh AK, Rawat M, Mani G, and others (2025) Postharvest physiology of mango crops: Understanding ripening, quality, and storage strategies. Appl Fruit Sci 67(2):1–14
18. Ntsoane ML, Zude-Sasse M, Mahajan P, and others (2019) Quality assessment and postharvest technology of mango: A review of its current status and future perspectives. Sci Hort 249:77–85
19. Wilson AD, Baietto M (2009) Applications and advances in electronic-nose technologies. Sensors 9(7):5099–5148
20. Voss HGJ, Stevan SL Jr, Ayub RA (2019) Peach growth cycle monitoring using an electronic nose. Comput Electron Agric 163:104858
21. Salunkhe RP, Patil AA (2015) Image processing for mango ripening stage detection: RGB and HSV method. In *Proceedings of the 2015 Third International Conference on Image Information Processing (ICIIP)*, 362–365. IEEE
22. Hasan BMS, Abdulazeez AM (2021) A review of principal component analysis algorithm for dimensionality reduction. J Soft Comput Data Min 2(1):20–30
23. Shah SSA, Zeb A, Qureshi WS, and others (2021) Mango maturity classification instead of maturity index estimation: A new approach towards handheld NIR spectroscopy. Infrared Phys Technol 115:103639

24. Busatto N, Vittani L, Farneti B (2022) and others. Physiological and molecular characterization of the late ripening stages in *Mangifera indica* cv. Keitt. *Postharvest Biology and Technology* 183: 111746
25. Surya Prabha D, Satheesh Kumar J (2015) Assessment of banana fruit maturity by image processing technique. J Food Sci Technol 52(3):1316–1327
26. Zakaria A, Shakaff AYM, Masnan MJ (2012) and others. Improved maturity and ripeness classifications of *Mangifera indica* cv. Harumanis mangoes through sensor fusion of an electronic nose and acoustic sensor. *Sensors* 12(5): 6023–6048
27. Tang H-Z, Ming J, Cheng Y-J, Zeng K-F (2010) Effect of degree of maturity on the volatile composition of mango fruits. Food Sci 31(16):247–252
28. Pathare PB, Opara UL, Al-Said FAJ (2013) Colour measurement and analysis in fresh and processed foods: A review. Food Bioprocess Technology.

Figures

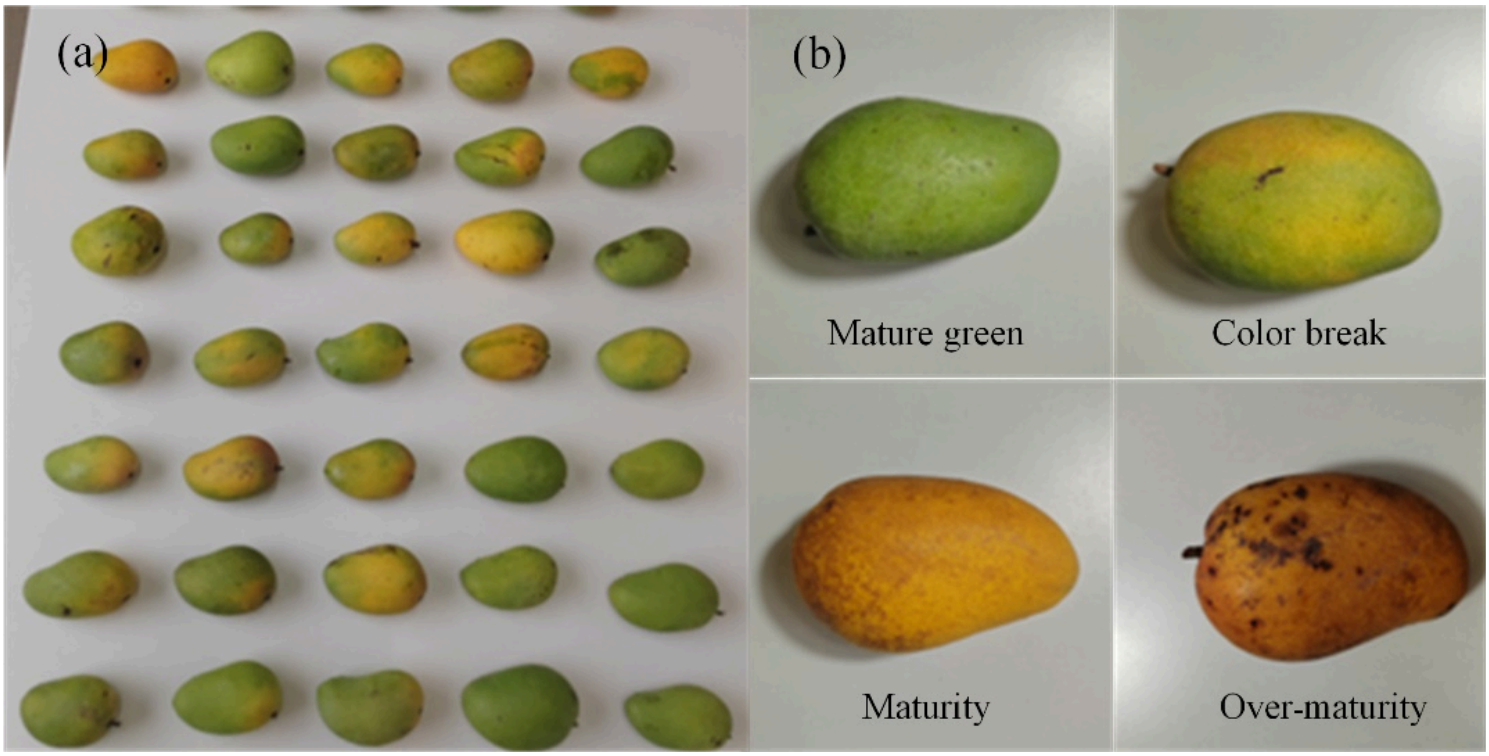


Figure 1

(a) mango sample image (b) different maturity stages mango image

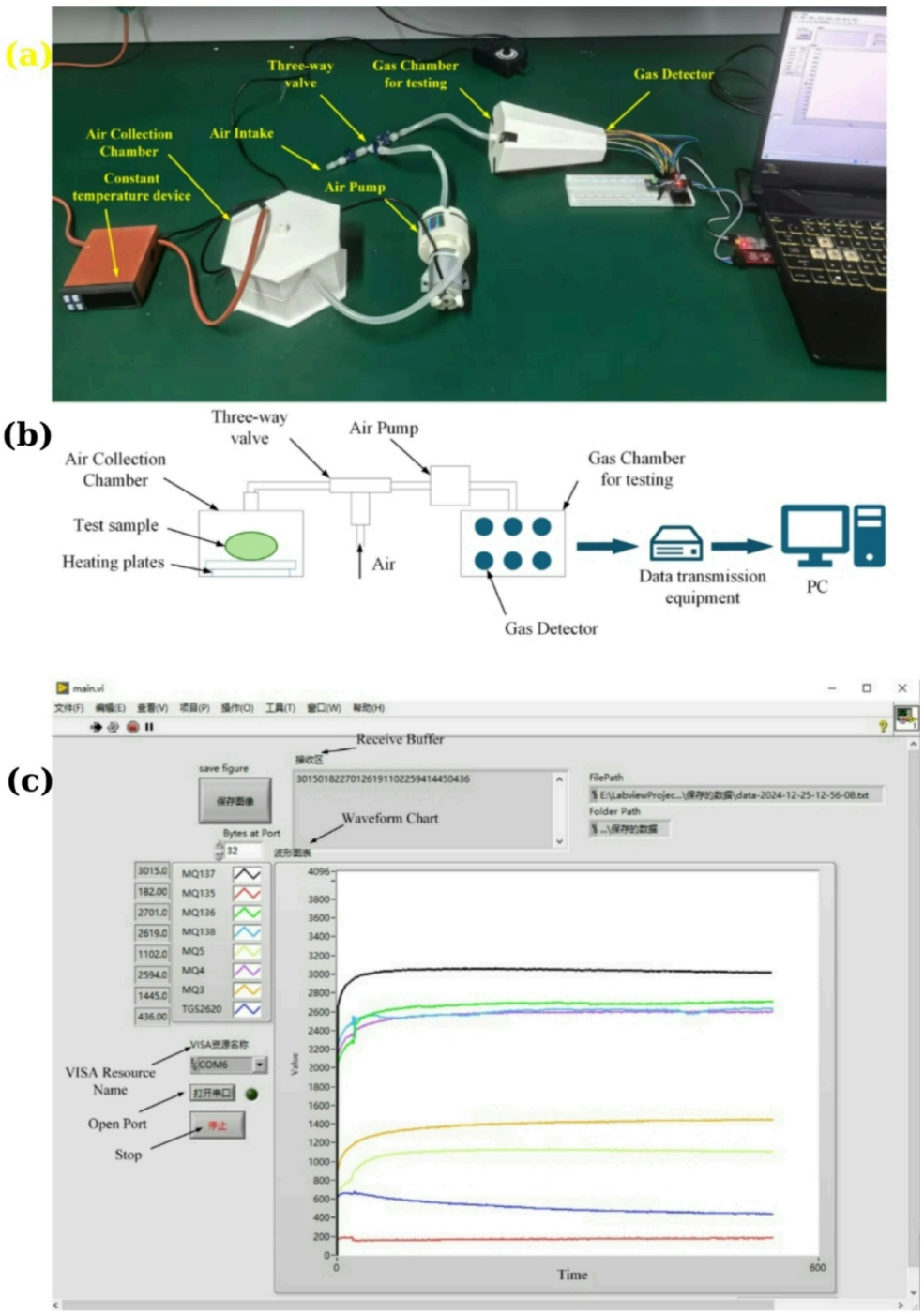


Figure 2

Self-made gas-sensing detection platform (a) gas-sensing test bench (b) gas-sensing flow diagram (c) real-time gas sensor monitoring GUI

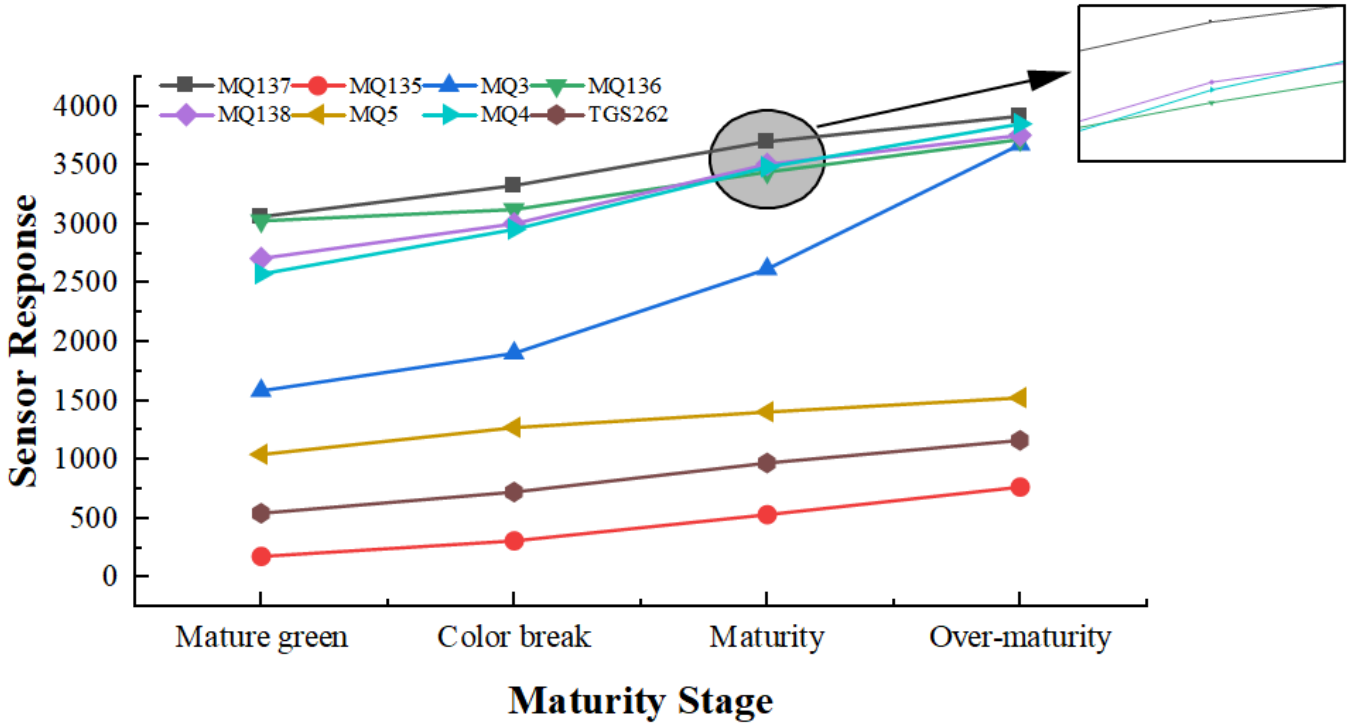


Figure 3

Gas sensors response in different maturity stages

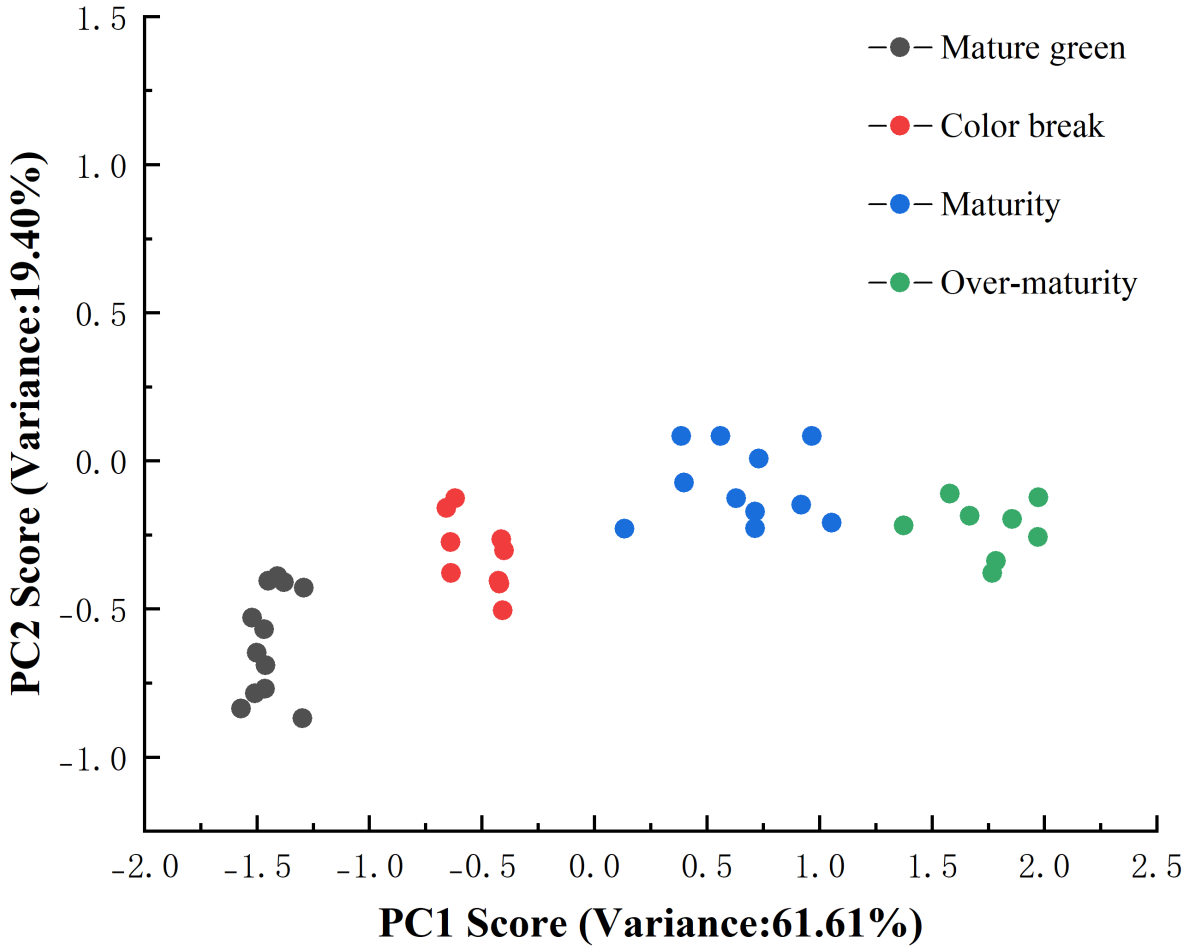


Figure 4

PC1-PC2 score scatter diagram for mango maturity stages